Applied Catalysis B: Environmental 180 (2016) 210–218

Contents lists available at ScienceDirect

Applied Catalysis B: Environmental

journal homepage: www.elsevier.com/locate/apcatb

Catalytic oxidation of trichloroethylene over Fe-ZSM-5: Influence of the preparation method on the iron species and the catalytic behavior

M. Romero-Sáez, D. Divakar, A. Aranzabal*, J.R. González-Velasco, J.A. González-Marcos

Group "Chemical Technologies for Environmental Sustainability", Chemical Engineering Department, Faculty of Science and Technology, Universidad del País Vasco/EHU, P.O. Box 644, E-48080 Bilbao, Spain

ARTICLE INFO

Article history:
Received 27 March 2015
Received in revised form 10 June 2015
Accepted 16 June 2015
Available online 23 June 2015

Keywords:
Cl-VOCs
Catalytic oxidation
Trichloroethylene
Fe-ZSM-5
Catalyst characterization

ABSTRACT

Fe-ZSM-5 zeolite was synthesized by following different routes namely ion exchange from solution, impregnation and solid state ion exchange. All the catalysts were tested in the oxidation of trichloroethylene (TCE) in vapor phase. The catalysts were characterized using different physico-chemical technique which included BET surface area analysis, NH_3-TPD analysis, H_2-TPR analysis, XRD analysis, TEM analysis, DRS UV–vis, EPR, and XPS. The characterization results gave significant insight on the active sites responsible for the oxidation. It was found that Fe nanoparticles present in the extra framework of the zeolite were largely responsible for oxidation rather than the acidic sites. The catalysts prepared by impregnation or solid state ion exchange method were found to be active in the oxidation of TCE; however, comprehensively less active than the catalyst synthesized by ion exchange method. The activity of Fe-ZSM-5 was also compared with H-ZSM-5, and it was found that the activity and stability of Fe-ZSM-5 catalyst was much higher than the protonic form. Studies on the deactivation mechanism of the catalysts showed that the major reason for loss in activity was due to formation of $FeCl_3$ rather than coke deposition.

1. Introduction

Iron exchanged zeolites have received much attention in recent years as catalysts for the removal of nitrogen oxides, especially by reduction of NO_x (NO and NO_2) with ammonia (SCR) [1], but also as $DeNO_x$ catalysts in lean-burn gasoline and diesel engines [2] and for N_2O decomposition [3]. Though Fe incorporated zeolites has been used for various oxidation applications [4], they have scarcely been applied for the oxidation chlorinated volatile organic compounds (Cl-VOCs), such as trichloroethylene. This pollutant can remain in ground water for a long time and get adsorbed in soil [5]. TCE is also one of the responsible components for depletion of stratosphere [6]. It is primarily used as organic solvent in industrial dry cleaning and degreasing and also present in adhesives, paint, and coatings [7].

Our pervious publication outlined that the incorporation of Fe improves the performance of the zeolite towards TCE oxidation and the synthesis procedure of Fe-zeolite can influence the activity of the catalyst [8]. In the literature, it has been reported that both the activity and hydrothermal stability of Fe-zeolites for NO_x reduction are influenced by several parameters including (i) zeolite topology, (ii) synthesis method, (iii) amount of introduced metal, and (iv) post-synthesis treatment. A variety of iron species and iron oxide clusters may also exist in the catalyst with a high degree of exchange [1]. On the other hand, the intrinsic activity of different iron species in the zeolite structure may differ depending on the structure, location, and electronic as well as steric environment around the active sites [9].

An extensive characterization of the catalyst has been carried out for better understanding the iron species present on the Fe-zeolites. Pérez-Ramirez et al. [10] exclusively studied the nature of Fe in zeolite system particularly ZSM-5 and beta, where iron was incorporated during the hydrothermal synthesis of the zeolite. A multiple characterization technique was followed to understand the physio-chemical change that occurred in Fe-zeolite on activation by calcination and stream treatment. They observed that zeolite structure plays an important role in the extraction of Al and Fe hetero atom from the framework positions. According to Delahay et al. [11,12], when Fe loading is low in the zeolite, mono nuclear iron-oxo cations are the predominant species and are highly active for reduction. However, on increasing the Fe content, binuclear iron-oxo species and iron oxides are formed which are not so active. Binuclear oxo-complex is found to be active towards SCR reaction [13] and N_2O direct decomposition [14]. In spite of abundant studies and although some well-supported hypotheses can be made, the exact structure of the active sites for NH_3-SCR in iron-zeolites remains unclear.

* Corresponding author. Fax: +34 946013500.
E-mail address: asier.aranzabal@ehu.es (A. Aranzabal).

http://dx.doi.org/10.1016/j.apcatb.2015.06.027
0926-3373/

In this work, Fe-ZSM-5 catalyst was synthesized by different routes namely ion exchange from solution, impregnation and solid state ion exchange, in order to obtain different superficial iron species and correlate the nature of these species with the catalytic activity in the oxidation of TCE. The nature and distribution of iron in the catalysts were determined by TEM, DR UV–vis, EPR, XPS, XRD, TPR, and TPD techniques and correlated with the catalytic performance.

2. Experimental

2.1. Preparation of Fe-zeolites

The zeolite NH_4-ZSM-5 with a Si/Al = 50 (CBV-5524G) was supplied from Zeolyst International. Fe was incorporated to the NH_4-ZSM-5 by three different procedures, namely wet ion exchange, solid state ion exchange, and impregnation, through the precursor salt $Fe(NO_3)_3{\cdot}9H_2O$. The amount of the salt and the zeolite were weighted previously so as to obtain a final catalyst with 2 wt.% Fe.

2.1.1. Wet ion exchange (IE)

Fe-ion exchange was carried out by dissolving $Fe(NO_3)_3{\cdot}9H_2O$ in water. NH_4-ZSM-5 was added to this solution (8 g L^{-1}) and was stirred for 24 h at 60 °C. The ion exchanged sample was then filtered, dried, and calcined at 650 °C for 4 h.

2.1.2. Solid state ion exchange (SSIE)

The solid iron salt ($Fe(NO_3)_3{\cdot}9H_2O$) was mechanically mixed and milled with the NH_4-ZSM-5 powder for 1 h and subsequently heated rapidly in an oven up to 500 °C at the rate of 50 °C min^{-1} and kept at the final temperature for an additional 1 h. The resulting sample was washed twice with deionized water and finally was calcined at 650 °C for 4 h.

2.1.3. Wet impregnation method (IMP)

The solid iron salt ($Fe(NO_3)_3{\cdot}9H_2O$) firstly was dissolved in water. Subsequently, the solution was slowly added to well stirred NH_4-ZSM-5 until the solvent was evaporated. The sample was then filtered, dried, and calcined at 650 °C for 4 h. The amount of Fe in the solution before and after was determined by ICP-AES to know the exact amount of Fe exchanged. In addition, solid samples were dissolved in a mixture of aqua regia, hydrofluoric acid, and nitric acid, and the resulting solutions were analyzed by AAS to confirm the amount of Fe in each zeolite.

2.2. Reaction conditions and experimental reaction set-up

The experimental reaction set-up is shown in Fig. 1. The feed consisted of dry compressed air stream, regulated by a gas mass flow controller (Bronkhorst High-Tech El-Flow F-201C-FAC-20-V), and a liquid stream of TCE dosed by mass flow controller (Bronkhorst High-Tech l-Flow L01-AAA-99-0-20S). The complete evaporation of the liquid stream and homogenous blend with the gas stream were carried out in a controlled evaporator mixer (Bronkhorst High-Tech CEM W-101A-111-K). The resulting gaseous stream was passed through the fixed catalytic bed inside a tubular quartz reactor, surrounded and heated by a convective-flow oven. An on-line gas chromatograph (Agilent Technologies 6890N) equipped with a HP-5 capillary column, and an micro electron capture detector (μ-ECD) was used to quantify the concentration of TCE in the reactor inlet and exit.

Before catalytic measurement, the fixed bed was dried at 200 °C during 2 h in pure N_2 flow (0.45 L_N min^{-1}). Catalytic tests were performed as light-off curve at atmospheric pressure by feeding constant total flow of 0.45 L_N min^{-1} with 1000 ppm of TCE and increasing temperature from 200 to 650 °C with a heating rate of 1.5 °C min^{-1} controlled by the thermocouple located in the entrance of the catalytic bed. The catalytic bed consisted of 850 mg (2 cm^3) of particulate catalysts (0.3–0.5 mm), resulting in a gas hourly space velocity (GHSV) value of 13,500 h^{-1}. These experimental conditions have been proven to prevent from mass transfer limitation: both Mears' and Weisz-Prater's criterions were satisfied [15].

On the other hand, the stability of Fe-zeolites in TCE oxidation has evaluated by exposing the catalyst for 980 min in stationary reaction conditions.

2.3. Characterization techniques

The transmission electron microscopy (TEM) images were obtained using a Philips CM200 (200 kV) transmission microscope, with a punctual resolution of 0.235 nm and lineal resolution of 0.144 nm. Sample preparation was required, which was carried out by suspending powder catalyst in a small amount of ethanol for 1 h, later it was dispersed with the aid of an ultrasonic bath. A few drop of this suspension was placed on the sample holder, which consists of a circular copper grid coated with a layer of amorphous carbon lattice.

The characterization by electron paramagnetic resonance spectroscopy (EPR) was carried out on powdered samples with a Bruker ELEXSYS 500 spectrometer equipped with a super-high-Q resonator ER-4123-SHQ, operating at X band. The magnetic field was calibrated by a NMR probe, and the frequency inside the cavity was determined with an integrated MW-frequency counter. Low temperature measurements were performed with a continuous flow helium cryostat. The temperature was stabilized with an Oxford Instrument (ITC 4) regulator.

Diffuse reflectance UV–visible spectroscopy (DR UV–vis) characterization was carried out in a Cary 5000 (1.2 version) spectrophotometer. Spectra were recorded at room temperature and in a wavelength range between 200 and 2500 nm.

X-ray photoelectron spectroscopy (XPS) spectra of the samples were recorded on a physical electronic spectrometer equipped with an analyzer 5701 PHI 10-360 and using a monochromatic radiation source Mg Kα. The C1s signal of adventitious carbon (284.8 eV) was used as internal standard for the determination of the position signal with a deviation of ±0.2 eV. The following regions were recorded: C1s, O1s, Al2p, Fe2p, Si2p, and depending on the case Cl2p. All deconvolutions of experimental curves were performed with Gaussian–Lorentzian distributions minimizing the value of $\chi 2$.

Temperature-programmed desorption (TPD) of ammonia was performed on a Micromeritics AutoChem 2910 instrument. Prior to adsorption experiments, the samples (80–90 mg) were first pretreated in a quartz U-tube under a nitrogen stream at 500 °C. Then, they were cooled down at 100 °C in a N_2 flow (20 cm^3 min^{-1}) before the ammonia adsorption started. The adsorption step was performed by admitting small pulses of ammonia in Ar at 100 °C up to saturation. Subsequently, the samples were exposed to a flow of argon (50 cm^3 min^{-1}) for 2 h at 100 °C in order to remove reversibly and physically bound ammonia from the surface. Finally, desorption was carried out from 100 to 550 °C at a heating rate of 10 °C min^{-1} in Ar stream (50 cm^3 min^{-1}). This temperature was maintained for 15 min until the adsorbate was completely desorbed. Since the acid strength is related with the amount of ammonia absorbed, it was determined by time integration of the TPD curves. All the samples showed two major desorption peaks. A desorption peak around 180–200 °C was considered as corresponding to weak acid sites, while the peak in the range 350–450 °C was considered as corresponding to strong acid sites [16].

Temperature-programmed reduction (TPR) analysis has been carried out in a Micromeritics AutoChem 2910 instrument, pro-

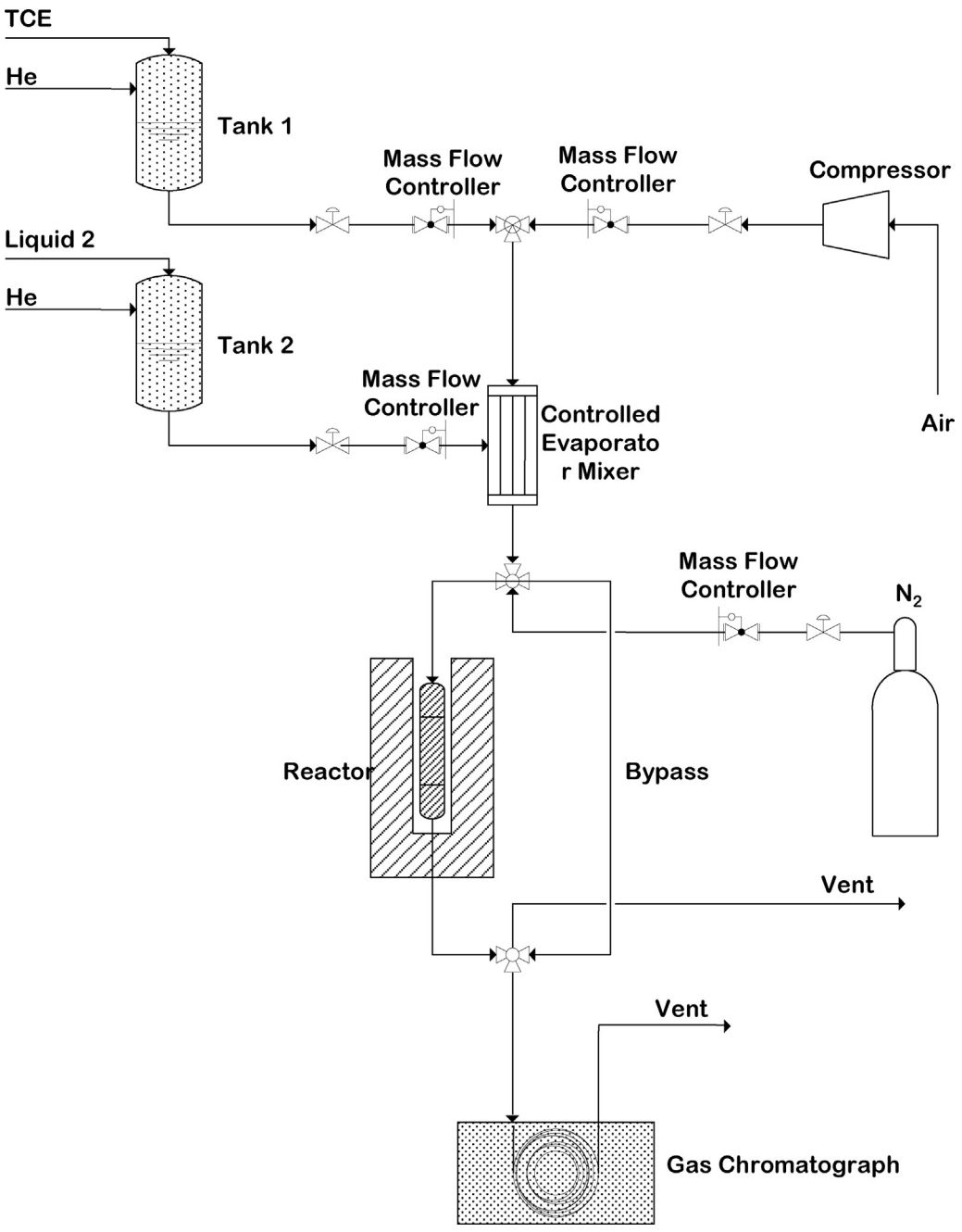

Fig. 1. The experimental set-up for the catalytic oxidation of TCE experiments.

vided with a thermal conductivity detector. The sample (0.08 g) was placed in a quartz U-tube, and was subjected to the following analysis sequence. Firstly, the catalyst was cleaned under a stream of Ar (50 cm^3 min^{-1}) and a temperature ramp of 10 °C min^{-1} from room temperature to 250 °C. The temperature was maintained at 250 °C for 1 h, and was lowered again to room temperature. The reducing gas used in all experiments was 5%H_2 in Ar, with a flow rate of 60 cm^3 min^{-1}. The temperature range explored was from room temperature to 900 °C with a heating rate of 20 °C min^{-1}. This temperature was maintained for 30 min so as to complete the reduction process. The water produced by reduction was trapped into a cold trap. The consumption of H_2 was qualitatively and quantitatively measured by time integration of TPR profiles.

X-ray diffraction (XRD) measurements have been made on a Philips diffractometer model PW1710, with Bragg–Brentano geometry, operating with Cu Kα radiation (λ = 1.541874 Å). Samples were scanned from 5° < 2θ <100°, and the X-ray diffraction line positions were determined with a step size of 0.02° and counting time of 1 s per step. The equipment is controlled by the X'pert Data Collector software. For the processing of the diffractograms and the identification of these phases PANalytical X'pert HighScore specific software has been used, in combination with the ICDD PDF2 database. The intensities of the peaks have been corrected to a value of fixed slit. In addition, the background from the diffractograms has been removed using the EVA program of the DiffracPLUS software package.

BET surface was evaluated from the nitrogen adsorption desorption isotherms, determined at −196 °C with a Micromeritics ASAP 2010 apparatus. The samples (100 mg) were outgassed at 350 °C for 16 h. The adsorption data recorded from the amount of

Table 1
Physicochemical properties for the fresh Fe-zeolites.

Catalyst	Fe content (wt.%)	S_{BET} ($m^2\ g^{-1}$)	Total acidity (mmol $NH^3\ g^{-1}$)	Weak acidity (mmol $NH^3\ g^{-1}$)	Strong acidity (mmol $NH^3\ g^{-1}$)	H_2/Fe
H-ZSM-5	–	411	0.286	0.103	0.183	–
Fe-ZSM-5, IE	1.88	356	0.201	0.109	0.092	1.1
Fe-ZSM-5, SSIE	1.84	340	0.228	0.115	0.113	1.1
Fe-ZSM-5, IMP	1.86	354	0.231	0.111	0.120	1.4

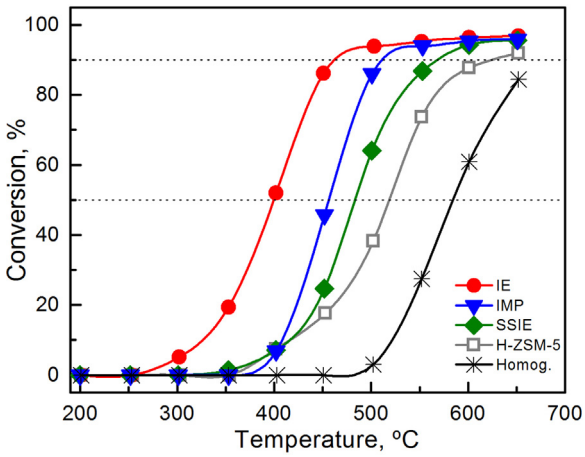

Fig. 2. TCE oxidation light-off curves over different Fe-ZSM-5 and H-ZSM-5 zeolite.

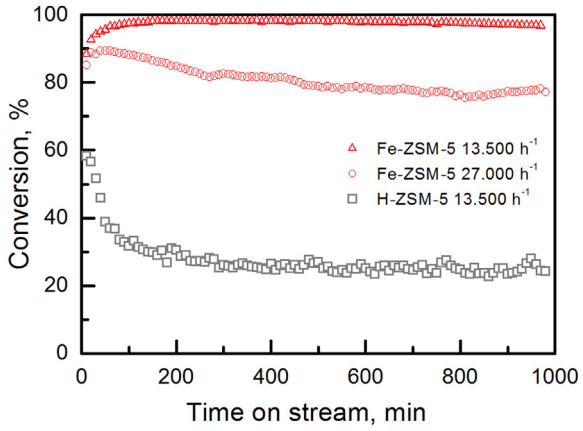

Fig. 3. Conversion of TCE vs. time on stream over Fe-ZSM-5 prepared by IE (13.500 and 27.000 h^{-1}) and H-ZSM-5 (13.500 h^{-1}).

N_2 physisorbed at different relative pressures were treated with the full BET equation.

3. Results and discussion

3.1. Characterization of textural properties

The Fe content, BET surface area and total acidity values of zeolites are listed in Table 1. The actual Fe loading was slightly less than the nominal loading in each catalyst because of the metal loss during washing. All Fe-ZSM-5 zeolites showed BET surface area values lower than obtained with H-ZSM-5. This happens because Fe particles added to its structure blocked some pores, reducing the access to the internal surface of these catalysts. The BET surface area values of the Fe-zeolites prepared by different methods differ by less than 4.5% among the prepared catalyst, indicating that the preparation method have little influence on this parameter.

On the other hand, the Fe incorporation reduces significantly the acidity of the catalyst, especially in the catalyst prepared by IE (30%). The acidity of the catalysts prepared by IMP and SSIE decreased around 20%. This is because the Fe can get exchanged at α, β or γ position in the zeolite, which in turn affects differently to the total acidity [17].

3.2. Activity of iron-zeolite catalyst prepared by different methods

Catalytic activity of Fe-zeolites in the oxidation of TCE was characterized by monitoring the conversion as function of temperature under above shown conditions. A characteristic curve, referred as ignition or light-off curve was obtained, as shown in Fig. 2. T_{50} and T_{90}, the temperatures at which 50 and 90% conversion was reached, respectively, were used as an indicative of relative reactivity of the catalysts. Each catalyst has been renamed with the name of the corresponding preparation method. The curves corresponding to reaction catalyzed by protonic zeolite and in the absence of catalyst are also included with the aim of comparison. It was found that the catalyzed reaction, regardless of the catalyst examined, occur at lower temperatures than the uncatalyzed reaction. Furthermore, it was also observed that the incorporation of iron into the H-ZSM-5 zeolite resulted in lower reaction temperatures for oxidation of TCE irrespective of the method of preparation used. Previous studies [16,18] showed that, the acidity of H-zeolites, especially Brönsted acidic centers, played a fundamental role in the oxidation of Cl-VOC, and the activity was directly related to its acidity. However, the lower acidity of Fe-zeolites suggests that the catalytic activity of the acidic centers is overcome by the redox properties of the iron centers.

As shown by Fig. 2, the Fe-zeolite prepared by IE showed better activity than the IMP counterpart, and both showed better results than sample prepared by SSIE method. T_{50} and T_{90} values for IE sample were about 395 and 460 °C, respectively. Meanwhile, the values of IMP sample were 60 °C higher (455 and 520 °C) and the results showed by SSIE catalyst were 85 and 110 °C higher (480–570 °C) compared to the IE sample. These differences in catalytic activity

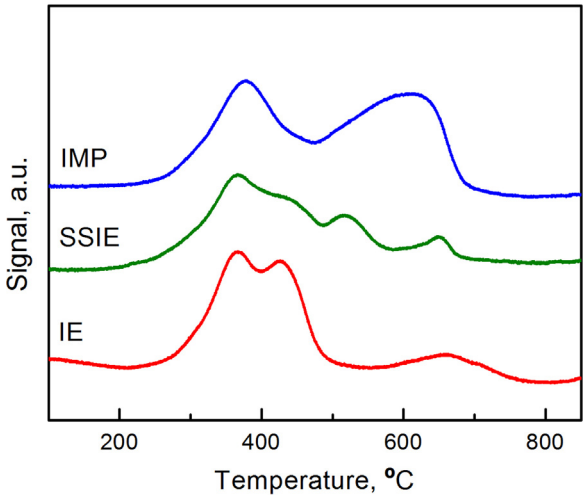

Fig. 4. H_2-TPR profiles of the Fe-ZSM-5 zeolites.

should be due to the formation of different iron species resulting from each particular preparation method of the catalyst.

Catalyst stability was also tested for the best sample (IE), subjecting the Fe-ZSM-5 catalyst operate for long on-stream periods at stationary conditions (0.85 g, 1000 ppm TCE, 0.45 L_N min^{-1}, 13,500 h^{-1}, 500 °C). As shown in Fig. 3, TCE conversion (ca. 100%) over Fe-ZSM-5 was kept constant with TOS, without deactivation. However, these experimental conditions did not allow to validate the catalyst is stable for long work-life, since it is unknown in which part of the catalytic bed complete conversion is reached, and thus which part of the catalytic bed is not working. Therefore, the experiment was repeated reducing the amount of catalyst in the bed to 0.425 g, and then increased the GSHV to 27,000 h^{-1}. A moderate and progressive deactivation with a decrease in the conversion from 90 to 81% was observed after 980 min of time-on-stream. However, H-ZSM-5 zeolite underwent rapid deactivation, within the first 100 min, to some lower residual conversion (20%), which is due to the loss of acid centers of protonic zeolites by coke formation and chlorine attack, as we reported previously [15,18]. This result supports the hypothesis raised above that redox properties of iron centers overcome the catalytic activity of acidic centers, and the iron centers are more stable. Therefore, the deactivation mechanism should be completely different.

The results showed so far indicate that the performance of Fe-ZSM-5 strongly depends on each particular sample, which is attributed to the impact of the preparation method on the catalyst constitution with respect to iron. In the section below each sample will be characterized in order to determine the nature of the iron species in each and find the most active species for the oxidation of TCE.

3.3. Characterization of iron species

With the aim to determine the nature of the iron species in each of the prepared catalyst and their relative reactivity in the oxidation of TCE, the prepared samples were analyzed through several techniques, such us, H_2-TPR, XRD, diffused reflectance UV–vis spectroscopy, EPR spectroscopy, and TEM.

The H_2-TPR profiles of Fe-zeolites reveal the reductive nature of Fe species. As shown in Fig. 4, H_2 consumption starts at 230–250 °C and concludes around 800 °C in all cases. 3 peaks were observed in the reduction of the catalyst prepared by IE. The first two, at 360 and 430 °C, showed greater intensity and have been attributed to the reduction of Fe_2O_3 to Fe^{2+} [19,20]. The splitting observed in this signal may be due to the different interaction of Fe_2O_3 with zeolite or its reduction in different location within the catalyst structure [21]. The third reduction signal, less intense, appeared around 660 °C, and corresponded to the reduction of Fe^{2+} to Fe^0. This Fe^{2+} corresponded to ions at extra-framework positions, since the reduction to metal iron of framework Fe^{2+} involves the collapse of the zeolite structure; then higher temperatures are required to achieve this reduction [22]. On the other hand, TPR of Fe-ZSM-5 prepared by SSIE had a similar profile as described above. The signal due to the reduction of Fe_2O_3 to Fe^{2+} also exhibited a splitting into two signals, centered at 360 and 440 °C. In this case, an additional signal at around 520 °C was found, corresponding to the reduction of

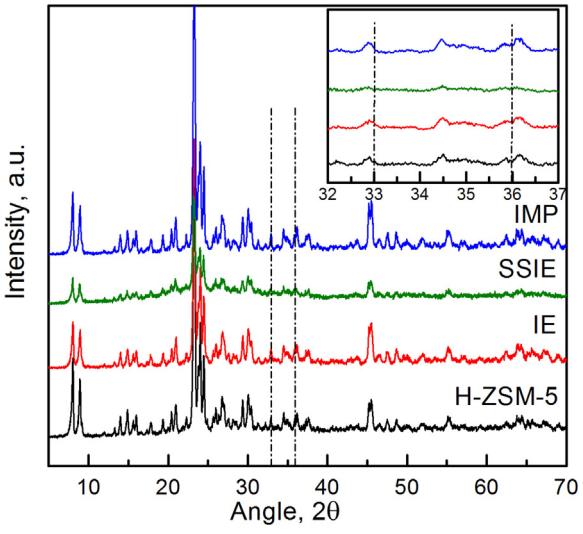

Fig. 5. XRD patterns of the Fe-ZSM-5 samples.

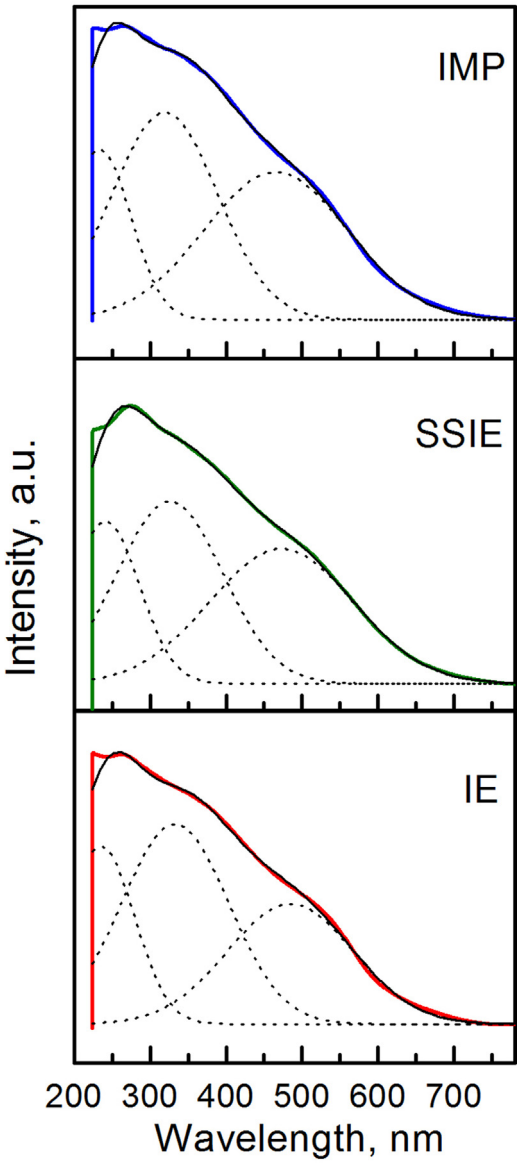

Fig. 6. DR UV–vis spectra and deconvoluted subbands of the Fe-ZSM-5 zeolites.

Table 2
Percentages of each band and their allocation to Fe^{3+} species obtained after deconvolution of the UV–vis spectra.

Catalyst	Fe^{3+}, isolated	$Fe(III)_xO_y$, clusters	Fe_2O_3, nanoparticles
Fe-ZSM-5, IE	16.7	46,5	36,6
Fe-ZSM-5, SSIE	24,5	44,1	31,3
Fe-ZSM-5, IMP	19,5	40,8	39,5

Table 3
Coke content and acidity of the fresh and used Fe-zeolites prepared by ion exchange in the oxidation of TCE.

Catalyst	Coke (%)	Total acidity (mmol NH_3 g^{-1})	Weak acidity (mmol NH_3 g^{-1})	Strong acidity (mmol NH_3 g^{-1})
Fe-ZSM-5 IE, Fresh	–	0.201	0.109	0.092
Fe-ZSM-5 IE, Used	0.3	0.225	0.164	0.037

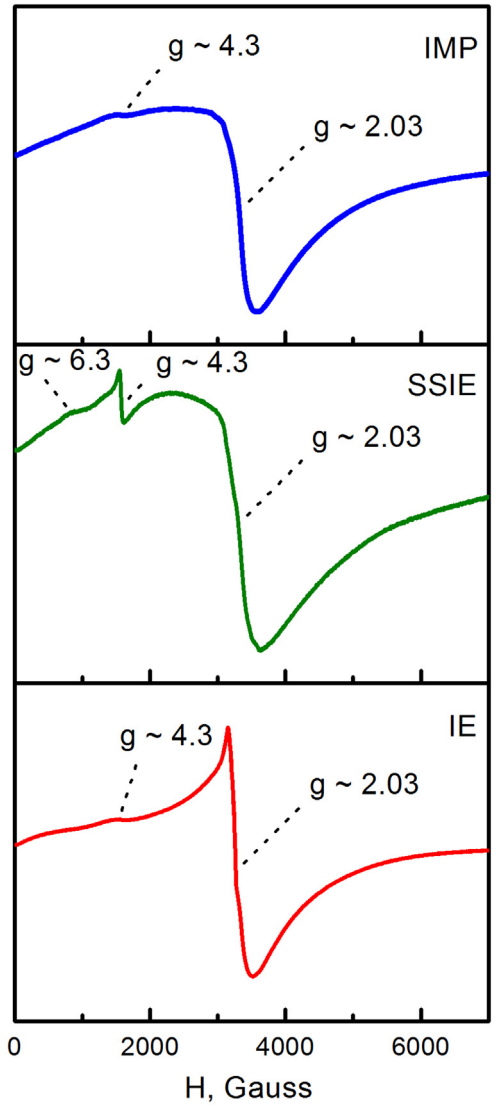

Fig. 7. EPR spectra, taken at 20 °C, of the Fe-ZSM-5 samples.

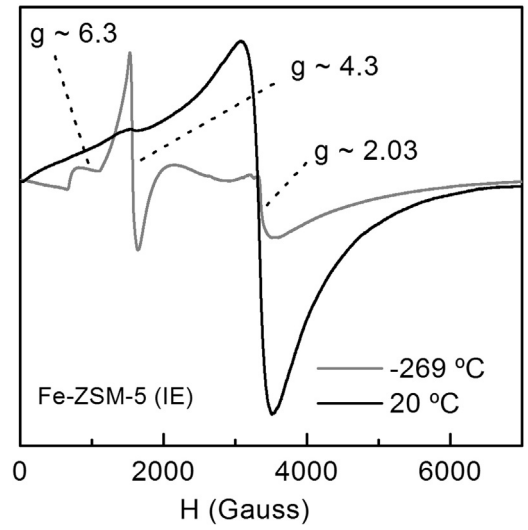

Fig. 8. EPR spectra of Fe-ZSM-5 zeolite prepared by IE at 20 and −269 °C.

Fe^{3+} present in different sites [23]. Finally, as in the previous case, a hump corresponding to the reduction of Fe^{2+} to Fe^0 also appeared at higher temperatures (650 °C). The samples prepared by IMP shows a different TPR profile from those obtained with the IE and SSIE catalysts, since in this case only two but very intense reduction signals were obtained. The first signal appeared around 375 °C, and corresponded to the reduction of Fe_2O_3 to Fe^{2+}. The second signal, that presented similar intensity than the first, appeared at about 660 °C and was due to overlap of transitions to magnetite (Fe_3O_4) to FeO and thence to Fe^0.

The integration of TPR curves allows the calculation of H_2/Fe ratios for each of the prepared catalysts. This parameter allows estimating the amount of iron present in Fe^{3+} oxidation state in the catalysts, as well as the degree of reduction suffered. According to the stoichiometry, a theoretical value of H_2/Fe equal to 1.5 indicates that all iron was incorporated as Fe^{3+}, and it was completely reduced to Fe^0; A H_2/Fe ratio of 0.5 is indicative of partial reduction of Fe^{3+} to Fe^{2+}; intermediate values (0.5–1.5) have been recorded in the literature of Fe-zeolites [24,25], as well as in the

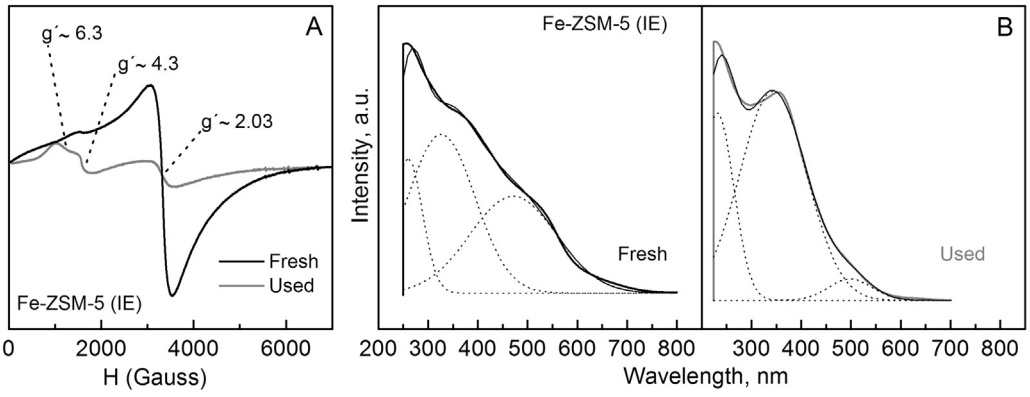

Fig. 9. Characterization of fresh and spent Fe-ZSM-5 zeolite prepared by IE. (A) EPR spectroscopy and (B) UV–vis spectroscopy.

three catalyst we have prepared. The catalyst prepared by IMP showed a ratio of 1:4, while the samples prepared by IE or SSIE the H_2/Fe showed a ratio of 1:1, which indicated that complete reduction to Fe^0 occurred to a lesser degree than in the former catalyst [26]. Though, Fig. 4 shows that the H_2 consumption over IMP catalyst occurred in a wider range of temperature (200–700 °C). This indicates that higher temperatures were needed to reduce part of the Fe species present in this catalyst. Something similar happened with the sample prepared by SSIE. However, the catalyst prepared by IE showed a large percentage (~90%) of hydrogen was consumed below 500 °C. This indicated that Fe species were more easily reducible, and therefore, they are more active at low reaction temperatures.

Fig. 5 shows the XRD diffractograms of the prepared Fe-zeolite samples, and the H-zeolite used as a reference. All samples exhibit the typical diffraction peaks of MFI structure, indicating that the crystalline nature of zeolites was maintained without any structural change after incorporation of Fe. Moreover, no peak indicating the presence of iron was observed. This absence of signal may be due to several factors such as the metal loading in the zeolite was low or their dispersion was high [27,28]. It is also possible that the diffraction peaks of α-Fe_2O_3 at 33 and 36° [29] are overlapped by the peaks of H-ZSM-5 at 32.87 and 36.15° [30].

The diffused reflectance UV–vis spectra of Fig. 6 show the Fe-ZSM-5 zeolites exhibited strong absorbance in 200–800 nm, revealing the existence of various ferric ion species in the samples. All spectra had similar profiles with overlapping signals of different intensity. Deconvolution of the strong signal was performed by the Origin8 software, using the fewest possible Gaussian bands and maximizing the quality of fit between the addition of these bands and the original signal. After the deconvolution of the spectra, the contribution of three characteristic UV–vis absorption bands was identified at 240, 350, and 500 nm. The bands around 250 nm are commonly assigned to isolated Fe(III) ions in tetrahedral or octahedral coordination [31,32]. The band located between 300 and 400 nm is ascribed to oligonuclear $Fe(III)_xO_y$ clusters in zeolite internal/external surfaces [10], and the band around 500 nm is attributed to Fe_2O_3 nanoparticles at the external surface of the zeolite crystal [33]. The integration of this Gaussian absorption bands allowed the estimation of the relative amount of Fe^{3+} species present in each catalyst, assuming the error due to the overlapping of these bands. As shown in Table 2, the main species were clusters of $Fe(III)_xO_y$, presenting almost the same percentage of Fe^{3+} in the form of clusters or nanoparticles. In all samples, isolated Fe^{3+} ions were minority species.

The EPR spectrum at room temperature of the Fe-ZSM-5 samples showed the presence of Fe^{3+}, irrespective of the method used in the catalyst preparation (Fig. 7). The observed signals at g' values of 2.03, 4.3, and 6.3, are common for Fe-ZSM-5 and also for Fe^{3+} ions in other oxide matrices [34,35]. However, the resolution of the spectra (measured by the narrowness of the peaks) was quite different, depending on the preparation method employed. The narrowest signal was at $g' \approx 2.03$, which is generally assigned to small clusters or Fe_2O_3 nanoparticles [36,37]. The sample prepared by IE showed a peak with higher resolution than other two catalysts. This means that the species responsible for this signal was distributed more evenly over the catalyst surface.

Isolated Fe^{3+} ions with high symmetry also contribute to the signals appearing at $g' \approx 2.03$ [14,38], so that their assignment in these conditions is unclear. On the other hand, the signals in the lower field region ($g' > 3$) are normally attributed to isolated Fe^{3+} ion in different coordination environments. Thus, signal at $g' \approx 4.3$ is normally assigned to Fe^{3+} ions incorporated in tetrahedral positions or isolated ions in extra framework positions [39,40], but sometimes this signal is also assigned to isolated Fe^{3+} ions in octahedral symmetry [41]. In any of the above cases, the symmetry of

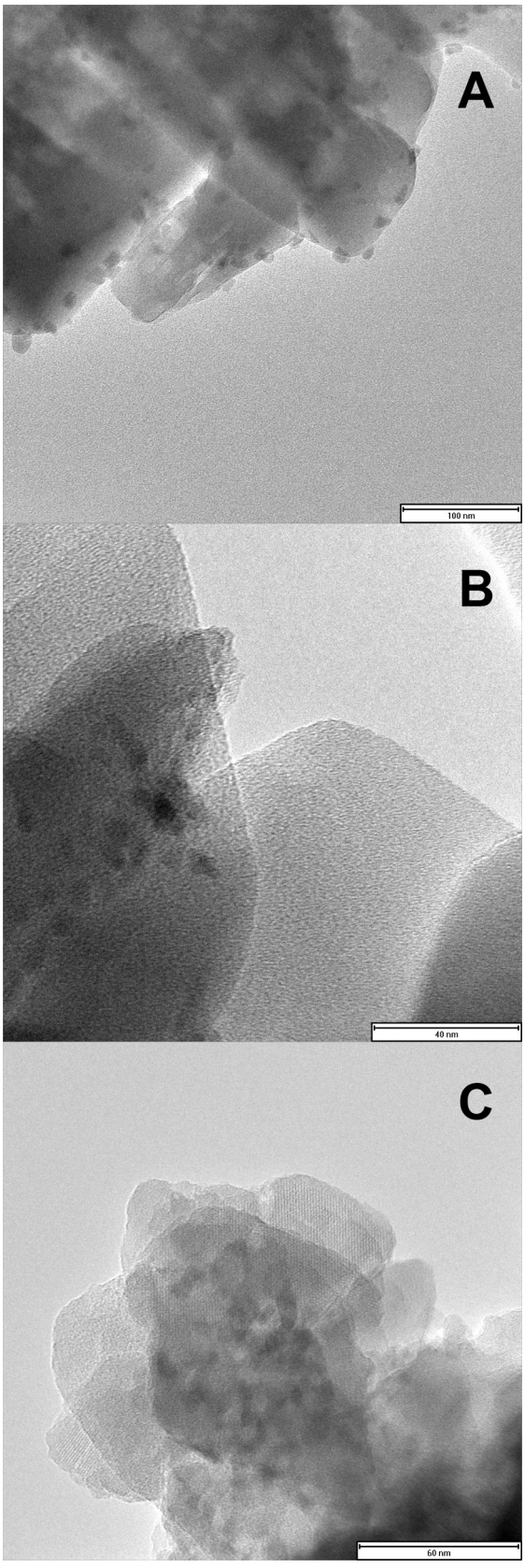

Fig. 10. TEM images of the Fe-ZSM-5 zeolites prepared by ion exchange (A), impregnation (B), and solid state ion exchange (C).

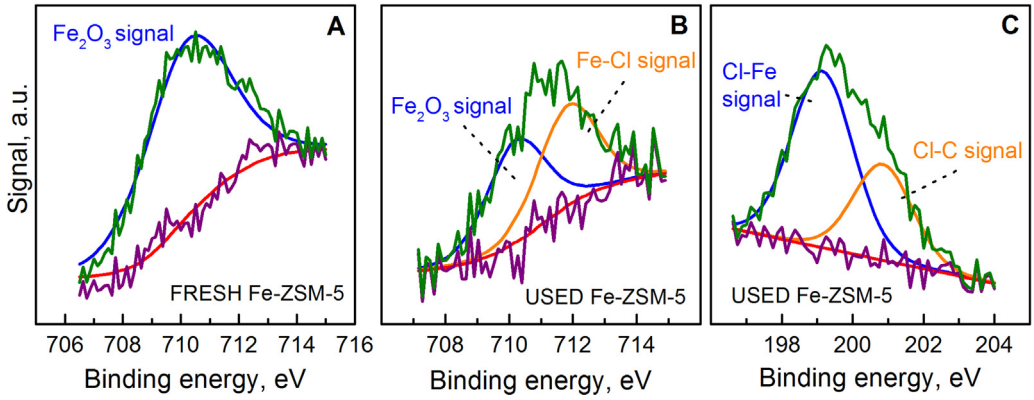

Fig. 11. XPS spectra and deconvoluted subbands of Fe-ZSM-5 zeolite prepared by IE. (A) Fe2p band of fresh catalyst, (B) Fe2p band of used catalyst, and (C) Cl2p band of used catalyst.

these ions presents axial distortion. Finally, the signal at $g' \approx 6.3$ is attributed to isolated Fe^{3+} species in higher coordination numbers and isolated rhombic distortion, normally in extra framework positions [40]. These signals were observed in all the EPR spectra; however, they are more clearly seen in the sample prepared by SSIE, because, in the other catalysts, the intensity of the signals at *gí* of 4.3 and 6.3 was diminished by the most intense signal at $g' \approx 2.03$. As mentioned above, the resolution of the spectra was different.

The discrimination between isolated ions and small groups of Fe_2O_3, as clusters or nanoparticles, in the signal at $g' \approx 2.03$ was resolved by the EPR analysis at low temperature. The isolated ions behave as Fe^{3+} paramagnetic species exhibiting narrow signals, whose intensity increases with decreasing temperature. In contrast, Fe_2O_3 nanoparticles and clusters cause broad signals at lower temperatures, which deviate from the paramagnetic behavior due to intrinsic antiferromagnetism [10]. Fig. 8 shows EPR analysis at 20 and −269 °C of the Fe-ZSM-5 zeolite prepared by IE. It was observed that at low temperatures the intensity of the signals at *gí* 4.3 and 6.3 increased, showing a clear paramagnetic behavior, characteristic of isolated ions. However, at low temperatures the intensity of the signal at $g' \approx 2.03$ suffered an important decline and its width is increased. This indicated that Fe^{3+} species responsible of this signal were linked through antiferromagnetic interactions inside clusters or particles, reducing the number of unpaired spins that contribute to the signal in EPR [42]. Therefore, the EPR analysis at −269 °C revealed that the signal at $g' \approx 2.03$ was due to clusters or nanoparticles of Fe_2O_3.

The spent catalysts were also characterized as shown in Fig. 9. EPR analyzes of the sample prepared by IE after reaction (Fig. 9A) showed that, the single peak suffered a decrease was the most intense, at $g' \approx 2.03$. Therefore, as explained above in the characterization of fresh catalysts, this indicated that the active iron specie in the oxidation of TCE were small groups of Fe_2O_3, as clusters or nanoparticles, and isolated Fe ions were not involved in the reaction.

On the other hand, the UV–vis analysis of the spent catalyst (Fig. 9B) showed a decrease in band centered at 500 nm relative to the other signals. As mentioned above, this band corresponds to Fe_2O_3 nanoparticles. However, by UV–vis was not possible to ensure that this was the only active species in this reaction, since the decrease of intensity that has suffered the band was in relation to the other two (centered at 250 and 350 nm). However, as the ratio of these two bands was maintained, and as by EPR we could see that isolated ions are not active in the reaction, it can be concluded that the active species in the TCE oxidation was Fe_2O_3 nanoparticles.

The size of Fe_2O_3 nanoparticles was measured by TEM microscopy. Fig. 10A shows a partial view of the Fe-ZSM-5 catalyst prepared by IE. The Fe_2O_3 nanoparticles are well distributed with an average size of 10 nm. TEM image of the sample prepared by IMP showed particles of similar size but with a low dispersion (Fig. 10B). Finally, the image of the Fe-ZSM-5 zeolite prepared by SSIE (Fig. 10C) shows Fe_2O_3 nanoparticles forming aggregates.

In view of the characterization results presented so far, it can be concluded that, the Fe-ZSM-5 catalyst prepared by IE, presents a greater dispersion of Fe_2O_3 nanoparticles (verified in the TEM analysis), a higher proportion of Fe^{3+} in the form of clusters-nanoparticles (concluded by UV–vis analysis), and a more uniform distribution of these two species of Fe^{3+} (shown by the higher resolution in $g' \approx 2.03$ in EPR signal). Therefore, the dispersion of the metal phase is a key factor to achive higher catalyst activity.

On the other hand, TPD-NH_3 analysis indicated that the acidity of these catalysts was not a determining factor in their activity, as the most active catalyst presented the lower acidity (Table 1).

The highest rate of deactivation of H-ZSM-5 is related the higher amount of coke (1.5 wt.%), and therefore, the severe decrease of strong acidity (Table 3) [15]. This type of acidity plays a key role in the activity and adsorption of chlorinated molecule in zeolites [8]. The amount of coke present on the Fe-ZSM-5 catalyst after 16 h of use was 0.3%. The amount of strong acid sites also decreased, but at lower extent. However, after reaction the weak acidity increased. This fact could be due to the formation of Fe-Cl species, as the $FeCl_3$ which is a Lewis acid [43,44].

To confirm the presence of $FeCl_3$ in the samples and see how the other components of the Fe-zeolites were affected during oxidation of TCE, XPS analysis of fresh and used catalyst were performed. As shown in Fig. 11A, the Fe 2p peak of fresh catalyst had only one signal at 710.2 eV, which corresponds to Fe_2O_3 [45,46]. In the characteristic chloride region of this catalyst, no signal was observed. However, in the Fe 2p peak of used catalyst (Fig. 11B), two different contribution were observed. One, at 710.2 eV, corresponds to Fe_2O_3 and the other signal, at 711.8 eV, corresponding to Fe—Cl bond which is due to the formation of $FeCl_3$ [47]. The presence of $FeCl_3$ in the catalyst explains the increase in weak acidity observed in TPD analysis of the used catalyst. Also, in the case of used catalyst the Cl 2p peak (Fig. 11C) had two different contribution. One at 199.1 eV corresponds to Cl—Fe bond, which supports the presence of $FeCl_3$ in catalyst. The second signal in this region, at 200.8 eV, attributed to Cl—C bonds, possibly present in coke produced during the reaction.

Therefore, XPS analysis of the fresh and used catalyst pointed to deactivation suffered by the Fe-zeolites was due to the combined effect of the loss of strong acidity and the formation of $FeCl_3$.

4. Conclusions

Zeolite supported iron catalysts (2 wt.% Fe-ZSM-5) were prepared by different methods in order to obtain catalysts with different Fe species. The nature and distribution of iron in the catalysts was determined by TEM, DR UV–vis, EPR, XPS, XRD, TPR. and TPD techniques and correlated with the catalytic performance in the oxidation of TCE, as a common Cl-VOC.

All the synthesized Fe-ZSM-5 zeolites exhibited higher activity than H-ZSM-5, though the most active as the sample prepared by ion exchange had the maximum activity. The EPR and UV–vis analyses of fresh and used samples showed that the active Fe species was Fe_2O_3 nanoparticles. By TEM analysis, it was found that the catalyst with highest activity was the one with a higher dispersion of Fe_2O_3 nanoparticles. Additionally, EPR analyses of fresh samples showed that the signal at $g' \approx 2.03$ corresponding to this catalyst was higher resolution than the prepared by other methods. This indicated that the size of clusters or nanoparticles in this catalyst were more uniform and had a greater dispersion in its surface. These results suggest that the higher number and better dispersion of Fe_2O_3 nanoparticles obtained by ion exchange were a key factor in its high activity.

NH_3 TPD analyses indicated that the acidity of these catalysts was not a key factor in their activity, since the catalyst which had the best activity was the one with a lower acidity. In addition, in the study of stability this catalyst lost 60% of its strong acidity after 980 min of operation, but continued to maintain very high conversion.

The stability of the Fe exchanged catalyst was found to be good, as the catalyst had high activity for long time on stream. By the characterization of used catalyst, it was determined that the loss of activity was due to the loss of acidity and the formation of $FeCl_3$ by chlorination of Fe_2O_3.

Acknowledgements

The authors wish to thank to the all the organizations that funded this research work: the Spanish Education and Science Ministry (Project CTQ2008-03551), the Basque Government trhough the Grant to Consolidated Research Groups (GIC-07/67-JT-450-07) and the University of the Basque Country UPV/EHU through the UFI (UFI 11/39). One of the authors (M.R.S.) acknowledges also to the Spanish Education and Science Ministry for the grant BES-2006-13729. The authors also kindly acknowledge the technical and human support from Advanced Research Facilities (SGIker), and specially the help of Professor Luis M. Lezama Diago from the Inorganic Chemistry Department of the Faculty of Science and Technology (U.P.V./EHU), in interpreting the EPR data, and Professors Concepción Herrera Delgado and Luis J. Alemany Arrebola from the Universidad de Málaga, in realization of the XPS analyses.

References

[1] S. Brandenberger, O. Kröcher, A. Tissler, R. Althoff, Catal. Rev. Sci. Eng. 50 (2008) 492–531.
[2] U. De La Torre, B. Pereda-Ayo, M. Romero-Sáez, A. Aranzabal, M.P. González-Marcos, J.A. González-Marcos, J.R. González-Velasco, Top. Catal. 56 (2013) 215–221.
[3] G. Moretti, G. Fierro, G. Ferraris, G.B. Andreozzi, V. Naticchioni, J. Catal. 318 (2014) 1–13.
[4] R. Gonzalez-Olmos, F.D. Kopinke, K. Mackenzie, A. Georgi, Environ. Sci. Technol. 47 (2013) 2353–2360.
[5] M. Mohseni, Chemosphere 59 (2005) 335–342.
[6] R. Gonzalez-Olmos, U. Roland, H. Toufar, F.D. Kopinke, A. Georgi, Appl. Catal. B – Environ. 89 (2009) 356–364.
[7] R.A. Parent, Encyclopedia of toxicology, in: P. Wexler (Ed.), Trichloroethylene, 2nd edition, Elsevier Academic Press, 2005, pp. 382–385.
[8] D. Divakar, M. Romero-Sáez, B. Pereda-Ayo, A. Aranzabal, J.A. González-Marcos, J.R. González-Velasco, Catal. Today 176 (2011) 357–360.
[9] A. Zecchina, M. Rivallan, G. Berlier, C. Lamberti, G. Ricchiardi, Phys. Chem. Chem. Phys. 9 (2007) 3483–3499.
[10] J. Pérez-Ramírez, J.C. Groen, A. Brückner, M.S. Kumar, U. Bentrup, M.N. Debbagh, L.A. Villaescusa, J. Catal. 232 (2005) 318–334.
[11] G. Delahay, M. Mauvezin, B. Coq, S. Kieger, J. Catal. 202 (2001) 156–162.
[12] G. Delahay, M. Mauvezin, A. Guzmán-Vargas, B. Coq, Catal. Commun. 3 (2002) 385–389.
[13] H.Y. Chen, T. Voskoboinikov, W.M.H. Sachtler, J. Catal. 180 (1998) 171–183.
[14] E.M. El-Malki, R.A. Van Santen, W.M.H. Sachtler, J. Catal. 196 (2000) 212–223.
[15] A. Aranzabal, M. Romero-Sáez, U. Elizundia, J.R. González-Velasco, J.A. González-Marcos, J. Catal. 296 (2012) 165–174.
[16] A. Aranzabal, J.A. González-Marcos, M. Romero-Sáez, J.R. González-Velasco, M. Guillemot, P. Magnoux, Appl. Catal. B – Environ. 88 (2009) 533–541.
[17] Q. Guo, B. Chen, Y. Li, J. Li, Catal. Lett. 120 (2008) 65–70.
[18] M. Gallastegi-Villa, A. Aranzabal, M. Romero-Sáez, J.A. González-Marcos, J.R. González-Velasco, Chem. Eng. J. 241 (2014) 200–206.
[19] N. Apostolescu, B. Geiger, K. Hizbullah, M.T. Jan, S. Kureti, D. Reichert, F. Schott, W. Weisweiler, Appl. Catal. B – Environ. 62 (2006) 104–114.
[20] A. Ates, Appl. Catal. B – Environ. 76 (2007) 282–290.
[21] L. Li, Q. Shen, J. Li, Z. Hao, Z. Ping Xu, G.Q. Max Lu, Appl. Catal. A – Gen. 344 (2008) 131–141.
[22] A. Guzmán-Vargas, G. Delahay, C. Bernard, Appl. Catal. B – Environ. 42 (2003) 369–379.
[23] A. Ates, A. Reitzmann, J. Catal. 235 (2005) 164–174.
[24] P. Balle, B. Geiger, S. Kureti, Appl. Catal. B – Environ. 85 (2009) 109–119.
[25] F. Heinrich, C. Schmidt, E. Loffler, M. Menzel, W. Grunert, J. Catal. 212 (2002) 157–172.
[26] H.Y. Chen, W.M.H. Sachtler, Catal. Today 42 (1998) 73–83.
[27] G. Qi, J.E. Gatt, R.T. Yang, J. Catal. 226 (2004) 120–128.
[28] Z. Liu, P.J. Millington, J.E. Bailie, R.R. Rajaram, J.A. Anderson, Micropor. Mesopor. Mat. 104 (2007) 159–170.
[29] G. Qi, R.T. Yang, Appl. Catal. A – Gen. 287 (2005) 25–33.
[30] M.M.J. Treacy, J.B. Higgins, Collection of Simulated XRD Powder Patterns for Zeolites, Elsevier, 2001.
[31] L. Capek, V. Kreibich, J. Dedecek, T. Grygar, B. Wichterlova, Z. Sobalik, J.A. Martens, R. Brosius, V. Tokarova, Micropor. Mesopor. Mater. 80 (2005) 279–289.
[32] S. Bordiga, R. Buzzoni, F. Geobaldo, C. Lamberti, E. Giamello, A. Zecchina, G. Leofanti, G. Petrini, G. Tozzola, G. Vlaic, J. Catal. 158 (1996) 486–501.
[33] P. Marturano, L. Drozdová, G.D. Pirngruber, A. Kogelbauerb, R. Prins, Phys. Chem. Chem. Phys. 3 (2001) 5585–5595.
[34] A. Brückner, R. Lück, W. Wieker, B. Fahlke, H. Mehner, Zeolites 12 (1992) 380–385.
[35] A.V. Kucherov, C.N. Montreuil, T.N. Kucherova, M. Shelef, Catal. Lett. 56 (1998) 173–181.
[36] D. Meloni, R. Monaci, V. Solinas, G. Berlier, S. Bordiga, I. Rossetti, C. Oliva, L. Forni, J. Catal. 214 (2003) 169–178.
[37] G. Catana, J. Pelgrims, R.A. Schoonheydt, Zeolites 15 (1995) 475–480.
[38] M.S. Kumar, M. Schwidder, W. Grünert, A. Brückner, J. Catal. 227 (2004) 384–397.
[39] A. Brückner, U. Lohse, H. Mehner, Micropor. Mesopor. Mater. 20 (1998) 207–215.
[40] D. Goldfarb, M. Bernardo, K.G. Strohmaier, D.E.W. Vaughan, H. Thomann, J. Am. Chem. Soc. 116 (1994) 6344–6353.
[41] J.W. Park, H. Chon, J. Catal. 133 (1992) 159–169.
[42] A.V. Kucherov, M. Shelef, J. Catal. 195 (2000) 106–112.
[43] J.W. Yoon, S.H. Jhung, D.H. Choo, S.J. Lee, J.S. Chang, Chem. Lett. 36 (2007) 1504–1505.
[44] A. Corma, H. García, Chem. Rev. 103 (2003) 4307–4365.
[45] A. Glisenti, G. Favero, G. Granozzi, J. Chem. Soc. Faraday Trans. 94 (1998) 173–182.
[46] E. Díaz, S. Ordóñez, A. Vega, A. Auroux, J. Coca, Appl. Catal. A – Gen. 295 (2005) 106–115.
[47] E.V. Golubina, E.S. Lokteva, V.V. Lunin, N.S. Telegina, A.Y. Stakheev, P. Tundo, Appl. Catal. A – Gen. 302 (2006) 32–41.